Article

Mineral-Assisted Pathways in Prebiotic Synthesis: Photoelectrochemical Reduction of Carbon(+IV) by Manganese Sulfide

Xiang V. Zhang, Scot T. Martin, Cynthia M. Friend, Martin A. A. Schoonen, and Heinrich D. Holland

More About This Article

Additional resources and features associated with this article are available within the HTML version:

- Supporting Information
- Access to high resolution figures
- Links to articles and content related to this article
- Copyright permission to reproduce figures and/or text from this article

View the Full Text HTML

Mineral-Assisted Pathways in Prebiotic Synthesis: Photoelectrochemical Reduction of Carbon(+IV) by Manganese Sulfide

Xiang V. Zhang,[†] Scot T. Martin,*,[†] Cynthia M. Friend,[†,‡]
Martin A. A. Schoonen,[§] and Heinrich D. Holland[∥]

Contribution from the Division of Engineering and Applied Sciences, Department of Chemistry & Chemical Biology, and Department of Earth and Planetary Sciences, Harvard University, Cambridge, Massachusetts 02138, and the Department of Geosciences, State University of New York, Stony Brook, New York

Received April 23, 2004; E-mail: smartin@deas.harvard.edu

Abstract: Photoelectrochemistry on mineral surfaces has the potential to play a central role in the prebiotic syntheses of building blocks for biomolecules. In this study, photoreduction of C(+IV) as bicarbonate is used as a probe to investigate the photoelectrochemical properties of alabandite (MnS) colloidal particles. Our experimental results show that photoreduction occurs and that formate is the initial photoproduct. A quantum efficiency of 4.2% is obtained (pH = 7.5). The quantum efficiency is temperature-independent from 298 to 328 K. In addition to formate, longer chain carbon products are also produced. Ion chromatography shows the presence of acetate and propionate. Infrared spectroscopy and mass spectrometry indicate the formation of longer chain organic molecules that contain oxygenated functional groups. Our results suggest that some prebiotic syntheses could have occurred via photoelectrochemical reactions on semiconducting minerals.

1. Introduction

How life started on early Earth more than 3.8 Ga ago is an intriguing and open question. Prebiotic synthesis, which is the conversion of simple inorganic and organic molecules into complex and biologically functional molecules, was the first step in the evolution of life. Complex reactions were necessary, including reactions that altered the oxidation state of carbon.[1] Reduced organic molecules served as the building blocks of amino acids and nucleotides. Our hypothesis is that photoelectrochemical reduction reactions at mineral surfaces may have efficiently promoted many of the reduction steps in prebiotic synthesis.

As an initial approach for evaluating the relevance of photoelectrochemistry to prebiotic synthesis, we report herein on the reduction of bicarbonate HCO_3^-(+IV) to yield formate $HCOO^-$(+II) and other reduced organic molecules. We employ the C(+IV) to C(+II) reduction reaction as a model for evaluating the importance of photoelectrochemistry in the broader class of reduction reactions of organic molecules, which lead to carbon−carbon coupling reactions and to the possible formation of aldehydes, ketones, and amino acids. The carbon−carbon coupling reactions are facilitated by the $CO_2^{•-}$ radical anion produced via CO_2 photoelectrochemical reduction. The reactive $CO_2^{•-}$ radical anion can lead to the formation of $HCOO^-$ or CO as stable products or alternatively to carbon−carbon coupling in products such as acetate CH_3COO^- or longer chain species.[2]

Although the pathways of C(+IV) to C(+II) carbon reduction reactions are not well understood, they have been hypothesized to occur on mineral surfaces.[3−6] Wächtershäuser[3,4] suggested the thermal reduction on pyrrhotite (FeS) by H_2S, a reaction that was supported by the observation that sulfur-containing organics (e.g., thiols) were produced.[7] Chen and Bahnemann[6] reported that acetic acid was formed when CO_2 was mixed with water and magnetite (Fe_3O_4) at 350 °C and 10 atm. The thermal reaction pathways, however, generally appear to require high temperatures, and the organic products at these temperatures might be thermally decomposed.[8]

In comparison, semiconductor minerals may be exceptionally active C(+IV) to C(+II) photocatalysts, even at moderate

[†] Division of Engineering and Applied Sciences, Harvard University.
[‡] Department of Chemistry & Chemical Biology, Harvard University.
[§] State University of New York, Stony Brook.
[∥] Department of Earth and Planetary Sciences, Harvard University.

(1) Orgel, L. E. *Proc. Natl. Acad. Sci. U.S.A.* **2000**, *97*, 12503−12507.

(2) Eggins, B. R.; Robertson, P. K. J.; Murphy, E. P.; Woods, E.; Irvine, J. T. S. *J. Photochem. Photobiol. A: Chem.* **1998**, *118*, 31−40.
(3) Wächtershäuser, G. *Proc. Natl. Acad. Sci. U.S.A.* **1990**, *87*, 200−204.
(4) Wächtershäuser, G. *Syst. Appl. Microbiol.* **1988**, *10*, 207−210.
(5) Cairns-Smith, A. G.; Hall, A. J.; Russell, M. J. *Origins Life Evol. Biosphere* **1992**, *22*, 161−180.
(6) Chen, Q. W.; Bahnemann, D. W. *J. Am. Chem. Soc.* **2000**, *122*, 970−971.
(7) Heinen, W.; Lauwers, A. M. *Origins Life Evol. Biosphere* **1996**, *26*, 131−150.
(8) Miller, S. L.; Bada, J. L. *Nature* **1988**, *334*, 609−611.
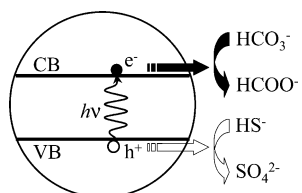
Figure 1. Schematic drawing of heterogeneous photoelectrochemical reduction of bicarbonate on semiconductor minerals.

temperatures. Their photoreducing ability is due to the conduction-band electrons formed during ultraviolet (UV) irradiation.[9] When a photon with an energy exceeding the band gap is absorbed, an electron (e^-) from the valence band (VB) is excited into the conduction band (CB). A hole (h^+) remains in the valence band (Figure 1). Semiconductors having a conduction band that is poised at a sufficiently negative voltage are thermodynamically capable of reducing carbon. The photoreduction of CO_2 to form $HCOO^-$ and CO has been reported when ZnS is irradiated with UV light.[10] CO_2 reduction upon UV irradiation of TiO_2[11,12] and other semiconductors[2,13] has also been reported.

Of the common semiconductors, ZnS and MnS have the important special property that their conduction bands are poised at the highly reducing positions, respectively, of -1.04 and -1.19 V versus the NHE (normal hydrogen electrode).[14] In comparison, the reduction potential of the $CO_2/HCOO^-$ half-reaction is -0.29 V. The large overpotential for carbon fixation by ZnS and MnS leads to the expectation of rapid photoreaction rates. The difference in band gap between ZnS (3.6 eV, 344 nm) and MnS (3.0 eV, 413 nm) suggests that MnS may use the solar spectrum more efficiently. Prior to this paper, however, there have been no reports concerning the photoelectrochemistry of MnS.

MnS is found in epithermal sulfide vein deposits and in anoxic laminated sediments. It is relatively rare in today's O_2-rich world. On early Earth, however, the absence of atmospheric O_2 and a more reduced mantle[15,16] decreased the prevalence of oxides and increased the occurrence of sulfides and carbonates. Furthermore, hydrogen sulfide from volcanic emissions and hydrothermal vents was abundant. Manganese accounts for 0.1 wt % of the Earth's crust.[17] For these reasons, on early Earth, MnS and $MnCO_3$ may have been abundant, possibly as colloids in the near-surface ocean euphotic zone.

We begin the study of MnS by using C(+IV) photoreduction as a general probe of the potential of MnS as a photoelectrochemically active mineral. A MnS aqueous colloidal suspension is irradiated with ultraviolet light in the presence of HCO_3^-
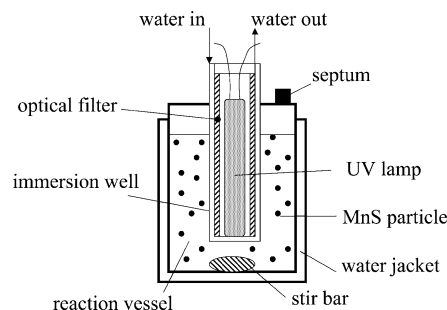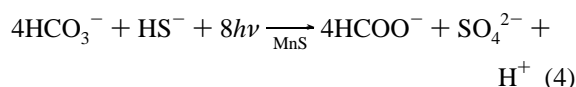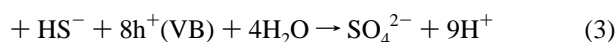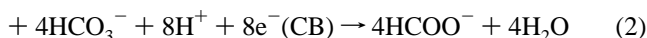
(9) Hoffmann, M. R.; Martin, S. T.; Choi, W. Y.; Bahnemann, D. W. *Chem. Rev.* **1995**, *95*, 69−96.
(10) Kanemoto, M.; Shiragami, T.; Pac, C. J.; Yanagida, S. *J. Phys. Chem.* **1992**, *96*, 3521−3526.
(11) Liu, B. J.; Torimoto, T.; Yoneyama, H. *J. Photochem. Photobiol. A: Chem.* **1998**, *115*, 227−230.
(12) Anpo, M.; Yamashita, H.; Ichihashi, Y.; Ehara, S. *J. Electroanal. Chem.* **1995**, *396*, 21−26.
(13) Inoue, T.; Fujishima, A.; Konishi, S.; Honda, K. *Nature* **1979**, *277*, 637−638.
(14) Xu, Y.; Schoonen, M. A. A. *Am. Miner.* **2000**, *85*, 543−556.
(15) Holland, H. D. *The Chemical Evolution of the Atmosphere and Oceans*; Princeton University Press: Princeton, NJ, 1984; pp 105−107.
(16) Kump, L. R.; Kasting, J. F.; Barley, M. E. *Geochem. Geophys. Geosyst.* **2001**, *2*, article 2000GC000114.
(17) Rudnick, R. L.; Fountain, D. M. *Rev. Geophys.* **1995**, *33*, 267−309.

Figure 2. Illustration of the photochemical apparatus.

and HS^-. MnS is thermodynamically capable of photoreducing bicarbonate through the following sequence:

$$8[MnS + h\nu \rightarrow e^-(CB) + h^+(VB)] \quad (1)$$

$$+ 4HCO_3^- + 8H^+ + 8e^-(CB) \rightarrow 4HCOO^- + 4H_2O \quad (2)$$

$$+ HS^- + 8h^+(VB) + 4H_2O \rightarrow SO_4^{2-} + 9H^+ \quad (3)$$

$$4HCO_3^- + HS^- + 8h\nu \xrightarrow{MnS} 4HCOO^- + SO_4^{2-} + H^+ \quad (4)$$

In the present work, the quantum efficiency of eq 4 is determined by using chromatographic analyses to quantify chemical species. Longer chain organic products, resulting from $CO_2^{\bullet-}$ carbon−carbon coupling reactions, are characterized by infrared spectroscopy and mass spectrometry. Compared to other common photocatalysts, such as TiO_2 and CdS, MnS is found to have significantly greater quantum efficiency, which is consistent with the highly reducing conduction-band electron.

2. Experimental Section

2.1. Characterization of MnS Particles. Commercially available $MnS \cdot (MnCl_2 \cdot 2H_2O)_{0.78}$ particles (Acros Organics, Geel, Belgium) were characterized by a combination of scanning electron microscopy (FEI Quanta 200) for particle size and shape, energy dispersion spectroscopy for bulk chemical composition, Rutherford backscattering spectrometry (1.7 MV General Ionex Tandetron ion accelerator) for chemical composition (100 nm depth), X-ray diffraction (XRD) (Scintag XDS2000) for existing crystalline forms, and ultraviolet−visible diffuse reflectance spectroscopy (Hitachi U-4001) for measuring light absorption properties.

2.2. Photochemical Apparatus. A commercial photochemical apparatus (ACE Glass, Vineland, NJ; Figure 2), consisting of a 0.5 L glass reaction vessel with a water jacket for temperature control (298−328 K with ±0.2 °C thermal stability), was used for all studies. A 450 W medium-pressure UV Hg arc lamp was encased in a quartz immersion well in the center of the reaction vessel. The apparatus was sealed tightly to exclude ambient O_2 from the reaction vessel, which otherwise would have oxidized MnS. The MnS suspension was constantly stirred during the UV irradiation. The light intensity from the UV lamp (200 nm < λ < 400 nm) was 2.2×10^{-5} M·s^{-1}, as measured by potassium iron(III) oxalate actinometry.[18]

2.3. Photochemical Reaction. Reaction mixtures were prepared in a nitrogen-filled glovebag. $MnS \cdot (MnCl_2 \cdot 2H_2O)_{0.78}$ (0.5 g) was added to 500 mL of deoxygenated water containing 7.2 mM NaHS and 2.5 mM $NaHCO_3$. The initial pH of the solution was 7.5. No change in pH occurred after the photoreaction. Following exposure to UV irradiation for a selected time period, 0.5 mL of solution was withdrawn from the reaction vessel through a septum and then forced through a

(18) Hatchard, C. G.; Parker, C. A. *Proc. R. Soc. (London)* **1956**, *A235*, 518.

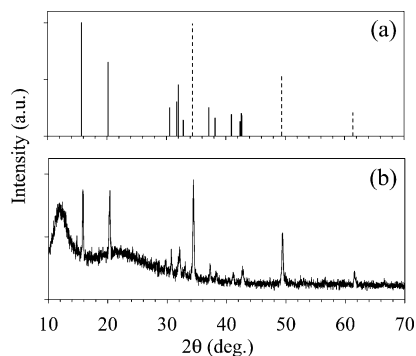**Figure 3.** X-ray diffraction (XRD) patterns. (a) Reference XRD patterns of α-MnS (dashed lines) and $MnCl_2\cdot2H_2O$ (solid lines).[40] (b) XRD measurement of $MnS\cdot(MnCl_2\cdot2H_2O)_{0.78}$ photocatalyst employed.

0.2 μm syringe filter as preparation for ion chromatographic, infrared, and mass spectrometric analyses.

2.4. Analysis of Photochemical Products. The loss of parent bicarbonate and the formation of photochemical products were determined by ion chromatography (Dionex DX120 with AS11-HC column). An eluent of 20 mM NaOH solution and a flow rate of 0.85 mL·min⁻¹ were employed for the detection of bicarbonate and formate. Sodium borate (5 mM) at a flow rate of 1.50 mL·min⁻¹ was the eluent for detection of acetate and propionate. A conductivity detector was used with self-regeneration suppression (SRS). The species in solution were identified by comparison to the chromatograms of pure chemicals. The concentrations were obtained by calibration with a series of standard solutions.

Transmission infrared spectroscopy (Nicolet Nexus 670) was used to characterize the chemical functionalities present in extractable products. After irradiation, the colloidal suspension was filtered, and 40 mL of the filtrate was extracted with 40 mL of CH_2Cl_2. The extract was concentrated to approximately 1 mL by rotary evaporation and subsequently evaporated to dryness on a silicon wafer. Infrared transmission spectra were recorded at 298 K with 512 scans at 4 cm⁻¹ resolution.

An aerosol mass spectrometer (AMS) was employed to characterize the chain length of organic products.[19,20] Reacted, filtered solution (40 mL) was aerosolized with a TSI 3076 atomizer. The aerosol particles were sampled through a critical orifice to create a particle beam. The particle beam was directed onto a resistively heated hot plate (ca. 350 °C), where the volatile and semivolatile constituents of the particle flash vaporized upon impact. The volatilized molecules were ionized by electron impact at 70 eV, and the positive ions of the fragments were passed through a quadrupole mass filter and detected as current at the electron multiplier.

3. Results and Discussion

3.1. Characterization of MnS Particles. The stoichiometry of the purchased powder is $MnS\cdot(MnCl_2\cdot2H_2O)_{0.78}$, as determined by a combination of Rutherford backscattering spectrometry and energy dispersion spectroscopy. This composition is further confirmed by digestion of the powder in 1.0 M H_2SO_4, followed by $[Mn^{2+}]$ analysis with flame atomic absorption spectroscopy and $[Cl^-]$ analysis by ion chromatography.

The crystal phases present in the purchased powder are determined by XRD (Figure 3). MnS has three known phases: α (green), β (pink), and γ (pink). The α phase is thermodynamically favored at both low and high temperatures; however,

(19) Jayne, J. T.; Leard, D. C.; Zhang, X. F.; Davidovits, P.; Smith, K. A.; Kolb, C. E.; Worsnop, D. R. *Aerosol Sci. Technol.* **2000**, *33*, 49−70.
(20) Katrib, Y.; Martin, S. T.; Hung, H. M.; Rudich, Y.; Zhang, H.; Slowik, J. G.; Davidovits, P.; Jayne, J. T.; Worsnop, D. R. *J. Phys. Chem. A* **2004**, in press.
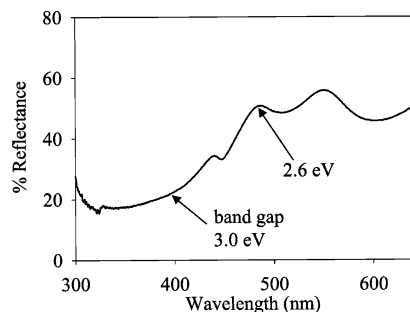
Figure 4. Ultraviolet−visible diffuse reflectance measurements of the MnS· $(MnCl_2\cdot2H_2O)_{0.78}$ photocatalyst at 298 K.

below 200 °C the metastable β and γ phases persist for kinetic reasons. The major XRD peaks of our MnS particles can be assigned to α-MnS, while the minor peaks of the dry powder are consistent with $MnCl_2\cdot2H_2O$. The broad peaks at 12° and 23° in Figure 3b are from the grease used to mount the powder sample. There are no unassigned residual peaks.

The onset of light absorption by the $MnS\cdot(MnCl_2\cdot2H_2O)_{0.78}$ particles is 475 nm based on UV−visible spectroscopy (Figure 4). This onset suggests a minimum band gap of 2.6 eV, which given the uncertainty in the measurement due to light scattering is consistent with the literature value of 3.0 eV.[14] The broad absorption tail may also be due at least in part to absorption by $MnCl_2\cdot2H_2O$ (pink color).

A distribution of particle diameters, with the most frequent diameter of approximately 1 μm, is observed by scanning electron microscopy (data not shown). These data are generally consistent with the particle size range provided by the vendor. The sedimentation rate of the turbid aqueous suspension is also consistent with micrometer-sized particles, which indicates an absence of extensive agglomeration in aqueous solution.

Although the dry powder is $MnS\cdot(MnCl_2\cdot2H_2O)_{0.78}$, a $[Mn^{2+}]$ and $[Cl^-]$ analysis of an aqueous suspension at pH = 7 shows, by stoichiometric balance of $2[Mn^{2+}]_{meas} \approx [Cl^-]_{meas}$, that the $MnCl_2$ is entirely soluble. Conversely, the percentage of MnS dissolution is less than 1%. We conclude that the aqueous suspension consists of micrometer-sized MnS particles suspended in a solution of $Mn^{2+}(aq)$ and $Cl^-(aq)$, which are in addition to the reactants $HCO_3^-(aq)$ and $HS^-(aq)$ and their products. (Thermodynamic calculations at pH = 7.5 show that $MnCO_3(s)$ is metastable compared to MnS(s) for our aqueous conditions. Calculations also show that MnS(s) is slightly undersaturated given $[Mn^{2+}]_{meas}$ and $[HS^-]_{meas}$; dissolution of 1% of the MnS(s) would lead to saturation.)

3.2. Photoreactivity.

3.2.1. Product Analyses. Formate and sulfate are produced when an aqueous MnS(s) suspension in the presence of $HCO_3^-(aq)$ and $HS^-(aq)$ is irradiated by UV light (Figure 5). Concomitantly, bicarbonate is lost.

Control experiments confirm that formate is generated from the heterogeneous photoreduction of bicarbonate at the MnS surface (Table 1). Specifically, no formate is detected in the absence of UV irradiation (control A), indicating dark thermal chemistry is not the mechanism for the reaction. Formate is not found if there is no MnS(s) present (control B) or in the presence of $Mn^{2+}(aq)$ alone (control C). These data demonstrate that there is no homogeneous photoreduction of bicarbonate. We find that HS^- is the electron donor (control D) and that bicarbonate is the electron acceptor (control E).
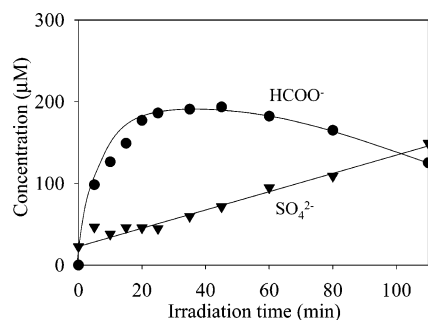
Figure 5. Concentration of reactants and products with increasing irradiation time at 298 K. The error bars are within the symbols. Conditions: 1 g/L MnS, 7.2 mM NaHS, 2.5 mM NaHCO$_3$, pH = 7.5, 298 K, and unfiltered radiation. Lines are drawn to aid the eye and do not represent a model fit.

Table 1. Control Experiments for Photochemical Reaction

description	UV? $\lambda < 410$ nm	catalyst? MnS (s)	hole scavenger? HS$^-$	electron acceptor? HCO$_3^-$	observation: formate?
			variables		
photochemical reaction	yes	yes	yes	yes	yes
control A	no	yes	yes	yes	no
control B	yes	no	yes	yes	no
control C	yes	no[a]	yes	yes	no
control D	yes	yes	no	yes	no
control E	yes	yes	yes	no	no

[a] No MnS(s) is present in control C. Instead, MnSO$_4$ is added at 6.3 × 10^{-4} M Mn^{2+}(aq).

In addition to formate, another possible primary product is carbon monoxide, which can be formed by the disproportionation[2] of two CO$_2^{\bullet-}$ radical anions to yield CO and CO$_3^{2-}$. We analyze the reactor headspace for CO using gas chromatography with thermal conductivity detection (GC-TCD). We find no CO, at least within the TCD detection limit. Although thermal conductivity is a relatively insensitive detection method, our measurements, nevertheless, set an upper limit of 10% yield for CO production from bicarbonate loss. Even though our results show that CO is not a major product pathway, given our sensitivity limits, CO production could still be an undetected minor pathway. For instance, CO production is reported as a minor product compared to formate for CO$_2$ reduction over ZnS.[10]

The temporal behavior of the aqueous formate concentration suggests complex product pathways (Figure 5). Formate concentration at first increases linearly, then stabilizes at 200 μM, and finally decreases to 120 μM at 110 min. After 2450 min, the formate concentration is 40 μM (not shown). In contrast, the sulfate concentration increases linearly, obtaining a concentration of 810 μM after 2450 min. Bicarbonate concentration over this time period decreases monotonically and is below the limit of our IC detection method after 2450 min. These linear changes in sulfate and bicarbonate suggest that they are the ultimate products and reactants, respectively. Formate, in contrast, appears to be a reactive intermediate.

If formate had a zero-order photochemical source and a first-order thermal sink, we would expect a steady-state concentration at sufficiently long time. The decrease in formate concentration beginning at 40 min thus suggests an intricate chemical mechanism. One explanation is that the CO$_2^{\bullet-}$ radical anion combines with formate (thus providing a second-order sink) to make longer chain products. These products may then compete

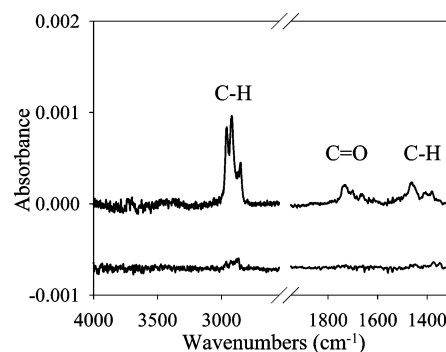**Figure 6.** Infrared spectra recorded for the CH$_2$Cl$_2$-extracted filtrate of reaction suspensions: (top) after 2450 min of irradiation; (bottom) prior to irradiation.

with HCO$_3^-$ for heterogeneous reaction sites on the MnS surface, which decreases the source of formate (i.e., no longer zero-order). Scavenging of conduction-band electrons also increases the concentration of long-chain organic radicals, which leads to further product formation. Sulfate may also competitively adsorb at the surface. The net result of decreasing the source of formate and increasing its sink is the reduction of formate concentration after an initial induction period. Ion chromatographic analysis of the irradiated solution after 2450 min finds 4 μM acetate and 15 μM propionate, which supports our proposed carbon−carbon coupling mechanism.

Infrared spectroscopy further supports this mechanism by demonstrating the production of reduced organic molecules after 2450 min (Figure 6). After UV irradiation, C−H and C=O vibrational modes are observed in a CH$_2$Cl$_2$-extract. (The fraction of organic molecules extracted from the original reacted aqueous solution by CH$_2$Cl$_2$ is unknown.) As a point of reference for interpretation of the observed spectra, the vibrational intensity of the C−H mode (2950 cm^{-1}) relative to that of the C=O mode (1730 cm^{-1}) is 0.20, 0.06, and 0.48 for formate, acetate, and propionate, respectively.[21] Although there is no definite trend between this ratio and the average oxidation state of the molecule, the relative C−H to C=O intensity of 4.4 in our product mixture suggests, nevertheless, that the molecules in the CH$_2$Cl$_2$-extract could be long chains (i.e., more C−H bonds) with relatively few C=O groups.

Aerosol mass spectrometry provides further evidence of long-chain organic molecules (Figure 7). After 2450 min irradiation, high mass fragments (100−300 amu) appear. The peak at 221 amu is consistent with a C$_{15}$ fragment; given the harsh electron impact ionization, the parent molecule undoubtedly has a longer chain length. There may also be fragments above 300 amu, which is the upper limit of the instrument's capability.

An analysis of mass balance provides additional support for the presence of carbon−carbon reaction products. After 20 min of photoreaction, 200 μM formate is produced, which corresponds to a 50−75% yield of measured bicarbonate loss. In contrast, after 2450 min formate is only 1−3% of bicarbonate loss. This difference at 20 min versus 2450 min supports a complex reaction mechanism, including carbon−carbon coupling products. Mass balance of sulfate concentrations also supports this mechanism. Under the limiting description of eq 4 (i.e., bicarbonate yields formate), the production of 810 μM sulfate after 2450 min implies the consumption of 3240 μM

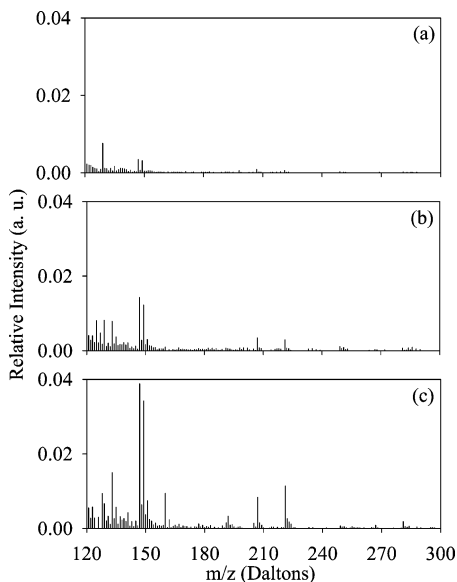(21) NIST Chemistry WebBook, http://webbook.nist.gov/chemistry/, 2003.

Figure 7. Mass spectra of solution components: (a) before irradiation; (b) after 110 min of irradiation; (c) after 2450 min of irradiation. Conditions are the same as in Figure 5.

Figure 8. Temperature dependence of formate production. Conditions are the same as in Figure 5. Lines are drawn to aid the eye and do not represent a model fit.

bicarbonate. This calculation is consistent with the observed depletion of bicarbonate at 2450 min because its initial concentration was 2500 μM. The "missing bicarbonate" of 740 μM implies electron acceptance by C(+II) species such as formate (cf. eq 4); therefore, the final average oxidation state must be closer to +I to balance the sulfate production. This decrease in oxidation state is consistent with the observation of carbon–carbon coupling products. As a result of these possible complex processes, many different organic molecules may form. After 2450 min, we have identified 40 μM formate, 4 μM acetate, and 15 μM propionate, whereas we expect a total of 2500 μM total organic carbon. This organic carbon is presumably tied up in the myriad combination of possible carbon–carbon long-chain molecules hinted at in the infrared and mass spectra: many organic molecules playing various roles in prebiotic syntheses could be present.

We can compare our results to those obtained for CO_2 photoreduction in ZnS suspensions.[10] Like MnS, ZnS is also highly photoreactive. Specifically, CO_2 photoreduction also occurs, and formate is generated with 2% quantum efficiency when HS^- is used as the electron donor. Two-carbon products such as oxalate are formed when tetramethylammonium chloride is added.[2] The products and quantum efficiencies vary depending upon pH, the type of electron donors, and the method of ZnS preparation. On the basis of these results for ZnS, we may infer similar dependencies for our results with MnS. Unlike our work with MnS, earlier work with ZnS has not reported long-chain carbon compounds, although it is unknown whether this absence is because these compounds were not formed or because they were not assayed. We hypothesize the latter.

3.2.2. Quantum Efficiency. Quantum efficiency is defined as the rate of product formation divided by the light intensity extinguished. Our experimental results show that the quantum efficiency of formate production is 4.2%. The quantum efficiency is a lower limit of the quantum yield (based on light absorbed) because light is partially extinguished due to scattering by the particle suspension. A quantum efficiency of 4.2% is significantly greater than values reported for other common
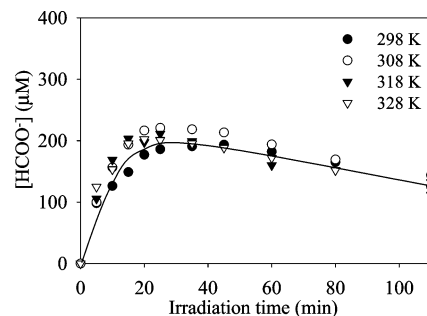
photocatalysts (e.g., TiO_2 or CdS). This observation is consistent with the highly reducing conduction-band electron of MnS.

We can compare the UV intensity of our experiments with that of early Earth. UV irradiation on early Earth is estimated as 6 W·m^{-2} (200 nm $< \lambda <$ 315 nm), which accounts for changes in solar luminosity and atmospheric chemical composition.[22] This UV intensity is 0.27% that of our Hg lamp in the same wavelength range. Generally, quantum efficiency increases slightly at lower light intensity.[23] The implication is that $\Phi =$ 4.2%, as employed by us in eq 5 (below), may be a lower limit.

3.2.3. Temperature Dependence. The production of formate is independent of temperature (Figure 8). Specifically, taking into consideration the reproducibility of separate experiments, there is no measurable change in the amount of formate produced at temperatures in the range of 298–328 K. Likewise, there is no temperature dependence in the concentrations of other species (mostly sulfur oxoanions), at least within the uncertainties of our measurements. The rates of thermal reactions often double for every 10 K change in temperature, whereas the rates of photochemical reactions are often temperature-independent. This further evidence of photochemical pathways corroborates our control experiments described for Table 1.

3.3. Photocorrosion. Valence-band holes may directly oxidize the sulfur of MnS instead of being scavenged by aqueous or surface-adsorbed electron donors. When this photocorrosion reaction occurs, Mn^{2+} and sulfur species are released into solution. Our data show that after irradiation of the MnS suspension (110 min, unfiltered UV radiation, 7.2 mM NaHS, and 2.5 mM NaHCO$_3$), the [Mn^{2+}](aq) increases by 150 μM, which corresponds to a loss of 3.6 mol % of the colloidal MnS(s) particles. The quantum efficiency for photocorrosion of MnS is thus estimated to be 0.008% for unfiltered light. The sulfur species released during photocorrosion may ultimately form sulfate and make a minor contribution to the time trend shown in Figure 5.

The long-term stability or renewal of MnS is important for sustainable photoelectrochemistry on early Earth. Our studies show that the efficiency of photocorrosion is 0.2% compared to carbon fixation. Although photocorrosion would have been important over the long time periods relevant to early Earth, there would also have been a continuous supply of H$_2$S and Mn^{2+}, in places such as near hydrothermal vents. Such an open

(22) Cockell, C. S. *Planet. Space Sci.* **2000**, *48*, 203-214.
(23) Kormann, C.; Bahnemann, D. W.; Hoffmann, M. R. *Environ. Sci. Technol.* **1991**, *25*, 494-500.

system differs from the closed system of our experiment, which contains a fixed amount of material. Hence, in the open system of early Earth, Mn^{2+} precipitation with H_2S might have continually renewed the availability of colloidal MnS.

3.4. Implications for Early Earth Carbon Fixation. A simple model (which is explained below) of MnS colloidal particles suspended in the euphotic zone of the early Earth ocean leads to the result that if there were 150 MnS particles cm^{-3} of 1 μm diameter, then the global carbon fixation due to photoreduction of CO_2 by MnS would have been competitive with that from other carbon sources. Our calculation assumes that the other endogeneous sources of fixed carbon ($C_{f,endo}$) total 5 × 10^9 mol·yr^{-1}, which has been suggested for an early Earth experiencing abundant electric discharges in a mildly reducing atmosphere with an H_2:CO_2 ratio of 1.[24] In comparison, the global carbon fixation due to photoreduction of CO_2 by MnS is modeled by us as follows:

$$C_{f,MnS} = IF\Phi \qquad (5)$$

where $C_{f,MnS}$ denotes the annual global carbon fixation by MnS colloidal photoelectrochemistry (moles·$year^{-1}$), I is the UV flux across the ocean of early Earth (einsteins·$year^{-1}$), F is the fraction of photons absorbed by MnS colloidal particles (200 nm < λ < 300 nm), and Φ is the quantum efficiency of formate production.

In eq 5 we use $I = 1.8 \times 10^{17}$ einsteins·yr^{-1}. This value is based on a UV flux on early Earth of 6 W·m^{-2} (200 nm < λ < 300 nm).[22] We assume a 90% fractional surface coverage by the ocean of early Earth.[25] We use a quantum efficiency of 4.2%, as measured in our laboratory experiments. Employing these values for I and Φ in eq 5, we conclude that if F is greater than 6.6×10^{-7}, then $C_{f,MnS} > C_{f,endo}$.

In our model of MnS colloidal particles suspended in the euphotic zone of an early Earth ocean, to estimate F we require the number concentration of the MnS colloidal particles (N, particles cm^{-3}) and their average diameter. We must also consider competition for the UV photons from seawater, ions, detrital particles, and organic material such as formate. The governing equation is

$$F = b_{abs}(MnS)/\Sigma b_{abs} \qquad (6)$$

where b_{abs} is the absorption coefficient. We consider UV absorption by pure seawater [b_{abs}(seawater) = 10 m^{-1} at λ = 200 nm[26]], Fe^{2+} [b_{abs}(Fe^{2+}) = 340 m^{-1} at λ = 260 nm and 9 × 10^{-4} M[27]], Mn^{2+} [b_{abs}(Mn^{2+}) = 0.0014 m^{-1} at λ = 245 nm and 80 μM[28]], HS^- [b_{abs}(HS^-) = 5.3 m^{-1} at λ = 260 nm and 100 μM[27]], detrital particulates [b_{abs}(detrital) = 0.013 m^{-1} at λ = 400 nm[29]], and formate [b_{abs}($HCOO^-$) = 0.69 m^{-1} at λ = 210 nm and 50 μM[30]].

The extinction coefficient (b_{ext}) of the MnS colloid is given by[31]

$$b_{ext} = (\pi/2)D_p^2 N \qquad (7)$$

We assume a 1 μm particle diameter (D_p); we also assume that the particles are black in the UV and hence $b_{abs} = b_{ext}$. Substitution of eq 7 into eq 6 shows that $N > 150$ particles cm^{-3} satisfies $F > 6.6 \times 10^{-7}$. When these conditions hold, photochemical processes involving MnS colloidal particles may have contributed significantly to prebiotic carbon fixation.

A further complication is that $MnCO_3$ is more common than MnS, at least on modern Earth. The likelihood of the presence of MnS versus $MnCO_3$ colloidal particles in the oceans of early Earth may be assessed by consideration of the equilibrium reaction:

$$MnS(s) + CO_2(g) + H_2O \rightleftharpoons MnCO_3(s) + H_2S, \ K = 1.1 \qquad (8)$$
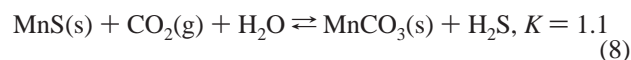
MnS is favored when $P_{H_2S}:P_{CO_2} > 1.1$. Current best estimates suggest $10^{-5} < P_{H_2S}:P_{CO_2} < 10^{-3}$ on early Earth.[15] We therefore conclude that in the open ocean $MnCO_3$ was likely more abundant than MnS. In regions of high H_2S concentrations, however, such as near hydrothermal vents, MnS colloidal particles may well have formed. A similar analysis for the stability of ZnS compared to that of $ZnCO_3$ shows that ZnS is favored for $P_{H_2S}:P_{CO_2} > 1.3 \times 10^{-12}$. ZnS colloidal particles may, therefore, have been more common than their MnS counterparts in the oceans of early Earth.

4. Conclusions

Our study shows that alabandite photoreduces bicarbonate to simple organic molecules such as formate, acetate, and propionate. The quantum efficiency is 4.2%. If MnS colloidal particles were present in sufficient concentration in the euphotic zone of the oceans of early Earth, they may have been a significant source of carbon fixation in the prebiotic world. MnS is also a constituent of meteorites,[32] which suggests photoelectrochemical synthesis reactions may also occur on extraterrestrial planets or on dust particles present in planetary nebulae.

Although we have specifically considered photoelectrochemical reduction of CO_2 on alabandite (MnS), the implications of our study are much broader: the key feature of photoelectrochemistry is the position of the conduction band, which produces electrons that are sufficiently energetic to induce the reduction of CO_2. Analogous carbon–carbon coupling reactions may also occur efficiently on other semiconductor minerals such as TiO_2, ZnS, CdS, and $FeTiO_3$. In contrast, similar reactions are not possible on iron sulfides because the conduction-band electrons are not sufficiently reductive.

The implications of our study are further broadened by noting that the CO_2 photoreduction reaction is a probe of the capability for more general chemistry, including carbon chain linking and the production of aldehydes, ketones, and carboxylic acids. Nitrogen fixation may also be induced by similar mechanisms. In the presence of carbon, nitrogen, and sulfur, production of amino acids or their analogues might possibly occur.[33] It is also

(24) Miller, S. L. The Endogenous Synthesis of Organic Compounds. In *The Molecular Origins of Life: Assembling Pieces of the Puzzle*; Brack, A., Ed.; Cambridge University Press: Cambridge, U.K., 1998; p 80.
(25) Galer, S. J. G. *Earth Planet. Sci. Lett.* **1991**, *105*, 214−228.
(26) Wells, N. *The Atmosphere and Ocean: a Physical Introduction*; Taylor & Francis: London, 1986.
(27) Cleaves, H. J.; Miller, S. L. *Proc. Natl. Acad. Sci. U.S.A.* **1998**, *95*, 7260−7263.
(28) Ferguson, J. *Prog. Inorg. Chem.* **1971**, *12*, 159.
(29) Morrow, J. H.; Chamberlin, W. S.; Kiefer, D. A. *Limnol. Oceanogr.* **1989**, *34*, 1500−1509.
(30) Optical properties of formate solution were measured in our laboratory.

(31) Seinfeld, J. H.; Pandis, S. N. *Atmospheric Chemistry and Physics: From Air Pollution to Climate Change*; Wiley-Interscience: New York, 1997.
(32) Lin, Y.; El Goresy, A. *Meteorit. Planet. Sci.* **2002**, *37*, 577−599.
(33) Reiche, H.; Bard, A. J. *J. Am. Chem. Soc.* **1979**, *101*, 3127−3128.

conceivable that semiconductor particles may have been employed in primitive photosystems of early organisms to harvest solar energy and synthesize organic molecules.

In agreement with this paper, other recent reports have also hypothesized the central role of minerals in prebiotic synthesis reactions. For example, porous rocks may have sheltered fragile early life forms from intense UV radiation.[34] Clay particles may have catalyzed the polymerization of RNA[35] and the development of cell membranes.[36] Borate minerals have been found to stabilize ribose.[37] Metals such as Fe, Mn, and Zn contained in rocks may have been the active centers of the earliest enzymes,

as suggested by an analysis of those occurring early in The Tree of Life.[38,39] Our study, which establishes a role for photoelectrochemistry in the production and transformation of organic molecules, contributes an additional mechanism by which minerals may have played a role in prebiotic synthesis.

(34) Hazen, R. M. *Sci. Am.* **2001**, 77.
(35) Ferris, J. P.; Ertem, G. *Science* **1992**, *257*, 1387−1389.
(36) Hanczyc, M. M.; Fujikawa, S. M.; Szostak, J. W. *Science* **2003**, *302*, 618−622.
(37) Ricardo, A.; Carrigan, M. A.; Olcott, A. N.; Benner, S. A. *Science* **2004**, *303*, 196−196.

(38) Osterberg, R. *Nature* **1974**, *249*, 382−383.
(39) Blankenship, R. E.; Hartman, H. *Trends Biochem. Sci.* **1998**, *23*, 94−97.
(40) JCPDS International Center for Diffraction Data; alabandite (06-0518), manganese chloride hydrate (72-0267); 1998.